Electronic Supplementary Material (ESI) for Nanoscale.

Supporting Information to:

Gated graphene islands enabled tunable charge transfer plasmon terahertz metamodulator

Arash Ahmadivand,†* Burak Gerislioglu,† Zeinab Ramezani‡

†*Department of Physics and Astronomy, Rice University, Houston, TX 77005, USA*

‡ *Electrical & Computer Engineering Department, Semnan University, Semnan, Iran*

**aahmadiv@rice.edu*

1. Graphene AC conductivity

In the current gate-controlled graphene-mediated metadevice, by setting the Fermi energy ($|E_F|$=95 meV) unchanged for interband transitions,[1,2] we only need to control the intraband transitions energy range. Therefore, the AC conductivity can be written as:[3]

$$\sigma_{AC}(\omega)=\left\{\left(\frac{-2ie^2k_{\mathrm{B}}T}{\pi\mathrm{h}^2\left(\omega-\frac{i}{\tau}\right)}\right)\log\left(2\cosh\left(\frac{E_{\mathrm{F}}}{2k_{\mathrm{B}}T}\right)\right)\right\} + \left\{\frac{e^2}{4\mathrm{h}}\left(f\left(\frac{\omega}{2}\right)+i\frac{2\omega}{\pi}\int_0^{\infty}\frac{f\left(\frac{\omega'}{2}\right)-f\left(\frac{\omega}{2}\right)}{\omega^2-\omega'^2}d\omega'\right)\right\} \tag{1}$$

where k_B is the Boltzmann constant, T is the room temperature (300 K), e is the electron charge, $\hbar$ is the reduced Planck's constant, and τ is the Drude relaxation rate, and $f(\omega)$ is:

$$f(\omega)=\frac{\sinh\left(\frac{\omega\mathrm{h}}{k_{\mathrm{B}}T}\right)}{\cosh\left(\frac{E_{\mathrm{F}}}{k_{\mathrm{B}}T}\right)+\cosh\left(\frac{\omega\mathrm{h}}{k_{\mathrm{B}}T}\right)} \tag{2}$$

In Equation 1, the first term explains the free-carrier intraband response of graphene islands (Drude-like conductivity), the second term gives the response based on the interband transitions (the nonzero conductivity at the charge neutrality point). Simplifying the Equation 1, the following equation indicates the employed graphene intraband conductivity as a function of frequency, with the applied voltage.[5] The result of this equation is a complex value, which is affecting both resistance and reactance of the system.

$$\sigma^{AC}_{\text{intraband}}(\omega)=\left(\frac{-ik_BTe^2}{\pi\mathrm{h}^2\left(\omega-\frac{i}{\tau}\right)}\right)\left(\frac{\mathrm{h}\nu_F\sqrt{\pi C_A\Delta V_{bg}}}{k_BT}+2\ln\left[1+e^{\frac{E_F}{k_BT}}\right]\right) \tag{3}$$

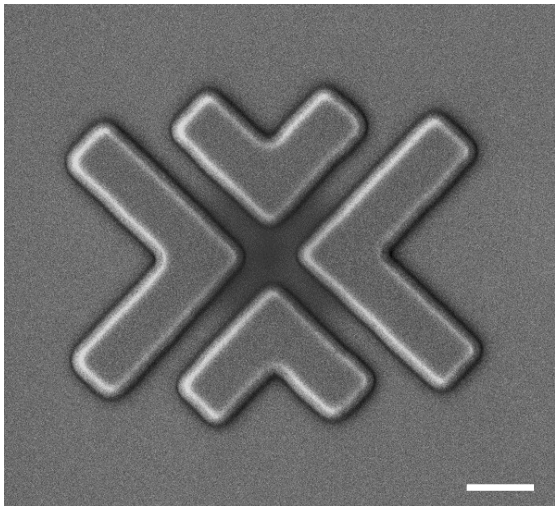

Figure S1. The SEM image of the graphene island-mediated metallic assembly. The scale bar is 5 μm.

The capacitance per unit area per charge of the substrate was set to C_A=8.45×10^{15}/m^{2}V.

2. Unit cell fabrication

The designed metallic assembly of V-shaped blocks were developed accurately by traditional photolithography on a multilayer substrate (SiO_2/ITO). We employed multilayer positive photoresists (PMGI and S1805) with the total thickness of 2 μm to develop the patterns. Utilizing the e-beam metallization tool, we then deposited 200 nm of Aluminium (Al) layer at the rate of 1 Å/s (pressure 3 × 10^{-4} mTorr). The unit cell arrays were fabricated in the area of 2×2 mm^2 with the periodicity of 25 μm. For the graphene layer-mediated metallic clusters, once the CVD graphene islands transferred (see Section 3) on the surface of the substrate, we carefully aligned the samples to constitute and adjust the planar two-dimensional metallic clusters on the graphene islands using the technique described in Ref. 6.

3. CVD graphene islands transfer and Raman spectroscopy

To develop graphene islands, a continuous, uniform, and atomically-thin layer of carbon was grown by CVD method utilizing CH_4 as the carbon source and Ar/H_2 as the carrier gas. We transferred the graphene monolayer onto a BaF_2 substrate covered with a thin layer of ITO by atomic layer deposition (ALD), then patterned into graphene islands with the diameter of 10 μm in arrays using e-beam lithography with poly(methyl methacrylate) (PMMA). We set the pressure, power, and duration of etching process (Oxygen

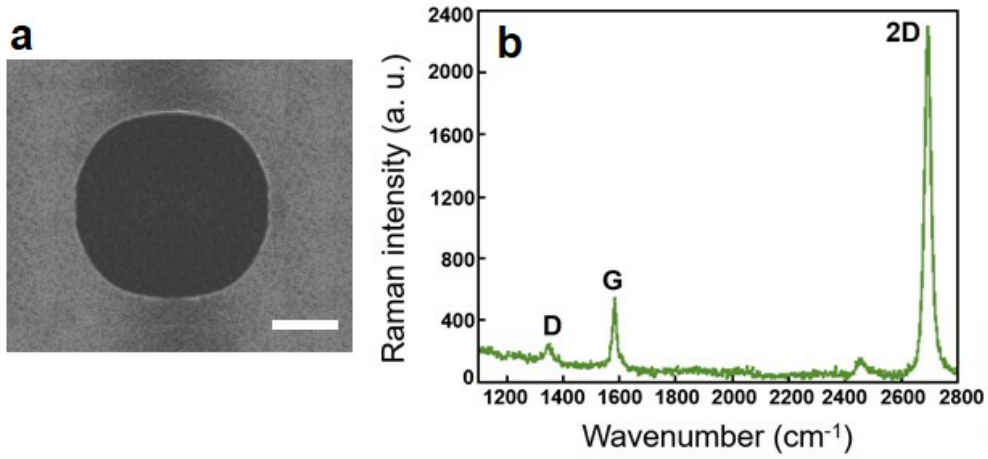

Figure S2. (a) Magnified SEM image of a graphene island. The scale bar is 2 μm. (b) Raman spectrum of the graphene monolayer with the corresponding setup parameters inside the profile.

plasma) to 500×10^{-3} Torr, 40 W and 15 seconds, respectively.[7] Figure S2a is a magnified SEM image of a graphene island before depositing aluminium samples. It should be noted that we employed the ITO layer as a conductive surface in direct contact with all graphene islands to provide charge injection and transition across the device gates and electrodes. On the other hand, in this set of experiments, Raman spectroscopy was performed on different areas of the fabricated metallic samples on top the graphene island, and the spectra show a distinct, narrow 2D extreme and low intensity D and G peaks with the ratio of D/G≈0.10, as plotted in Figure S2b.

4. THz-Time Domain Spectroscopy (THz-TDS) Setup

The THz characterization was performed using a THz time-domain spectroscopy (THz~TDS) setup with the beam bandwidth of *f*~1 THz to 5 THz, the frequency resolution of 200 GHz, and a signal-to-noise (*S/N*) ratio of over 10,000:1. Figure S3 shows the applied TDS signal amplitude as a function of time delay. More precisely, for the generation of broadband THz beams, we used a Ti:Al_2O_3 femtosecond oscillator with the pulse width of 100 fs. The dominant wavelength and average power of the oscillator were set to 850 nm and 1.5 W, respectively. The pulsed laser beam was focused onto a biased GaAs THz emitter. The propagating terahertz radiation was detected electro-optically using a ZnTe crystal.

5. Numerical analysis

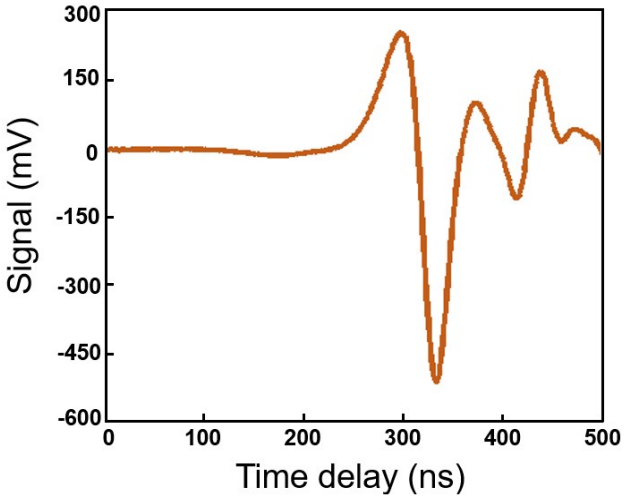

Figure S3. The applied incident signal in the THz-TDS setup as a function of time delay.

FDTD simulations. To predict and study the electromagnetic response of the THz-CTP resonant device in the presence of graphene islands, we used FDTD numerical (Lumerical 2018 package) to solve Maxwell's equations. For the optical computations, the simulation area discretization was set to d_x=d_y=15 nm in *x*- and *y*-planes, and d_z=0.01 nm in *z*-axis. Perfectly matched layer (PML) boundaries with 26 layers along the beam propagation direction (z-axis) and symmetric–antisymmetric periodical boundaries were employed for *x*- and *y*-trajectories. To satisfy the Courant stability, we set the simulation time step to *dt*~ 0.1 fs.

To determine the electrical properties and doping of graphene islands, we quantified the carrier lifetime based on experimentally demonstrated results in Ref. [8] for the mobility (2100 cm^2 /V.s). To determine the electrical properties of the developed THz-CTP resonant device, we employed typical parallel-plate capacitor model. Using this approach, we determined and predicted the initial *n*-doping of the graphene to be ≈ 6.8×10^{11} cm^{-2}, corresponding to a zero-bias Fermi level of $|E_F|$≈95 meV.

FEM simulations. To compute and plot the charge density maps and E-field snapshots, we employed FEM tool (COMSOL Multiphysics 5.3a) with the RF module by implementing Gauss's Theorem at the surface of the gated graphene islands-mediated metallic assemblies.

References

1. F. Valmorra, G. Scalari, C. Maissen, W. Fu, C. Schönenberger, J. W. Choi, H. G. Park, M. Beck, J. Faist, Low-bias active control of terahertz waves by coupling large-area CVD graphene to a terahertz metamaterial, *Nano Lett.* 13, 3193-3198 (2013).

2. F. Xiao, W. Zhu, W. Shang, T. Mei, M. Premaratne, J. Zhao, Electrical control of second harmonic generation in a graphene-based plasmonic Fano structure, *Opt. Express* 23, 3236-3244 (2015).

3. G. W. Hanson, Dyadic Green's functions and guided surface waves for a surface conductivity model of graphene, *J. Appl. Phys.* 103, 064302 (2008).

4. B. Sensale-Rodriguez, R. Yan, M. M. Kelly, T. Fang, K. Tahy, W. S. Hwang, D. Jena, L. Liu, H. G. Xing, Broadband graphene terahertz modulators enabled by intraband transitions, *Nat. Commun.* 3 780 (2012).

5. J. Kim, H. Son, D. J. Cho, B. Geng, W. Regan, S. Shi, K. Kim, A. Zettl, Y. –R. Shen, F. Wang, Electrical control of optical plasmon resonance with graphene, *Nano Lett.* 12, 5598-5602 (2012).

6. D. Schurig, J. J. Mock, and D. R. Smith, Electric-field-coupled resonators for negative permittivity metamaterials, *Appl. Phys. Lett* 88, 041109 (2006).

7. X. Liang, Z. Fu, and S. Y. Chou, Graphene transistors fabricated via transfer-printing in device active-areas on large wafer, *Nano Lett.* 7, 3840-3844 (2007).

8. F. H. L. Koppens, T. Mueller, P. Avouris, A. C. Ferrari, M. S. Vitiello, M. Polini, Photodetectors based on graphene, other two-dimensional materials and hybrid systems, *Nat. Nanotechnol*. 9, 780-793 (2014).